

# Along-shelf hydrographic anomalies in the Nordic Seas (1960–2011): locally generated or advective signals?

Vidar S. Lien · Yvonne Gusdal · Frode B. Vikebø

Received: 30 September 2013 / Accepted: 14 May 2014 / Published online: 7 June 2014  
© The Author(s) 2014. This article is published with open access at Springerlink.com

**Abstract** The northward flow of warm and saline Atlantic Water through the eastern Nordic Seas sustains a spring-bloom ecosystem that hosts some of the world's largest commercial fish stocks. Abrupt climatic changes, or changes beyond species-specific thresholds, may have severe effects on species abundance and distribution. Here, we utilize a numerical ocean model hindcast to explore the similarities and differences between large-scale anomalies, such as great salinity anomalies, and along-shelf hydrographic anomalies of regional origin, which represent abrupt changes at subannual time scales. The large-scale anomalies enter the Nordic Seas to the south and propagate northward at a speed one order of magnitude less than the Atlantic Water current speed. On the contrary, wind-generated along-shelf anomalies appear simultaneously along the Norwegian continental shelf and propagate northward at speeds associated with topographically trapped Kelvin waves. This process involves changes in the vertical extent of the Atlantic Water along the continental slope. Such a dynamic oceanic response both affects thermal habitats and has the potential to ventilate shelf waters by modifying the cross-shelf transport of nutrients and key prey items for early stages of fish.

**Keywords** Atlantic water · Basin-shelf exchange

## 1 Introduction

The heat content and water mass characteristics of the Nordic Seas are controlled by the inflow of warm and saline Atlantic Water (AW) in the southeast (e.g., Hansen and Østerhus 2000) and cold and less saline Arctic-influenced water masses in the northwest (e.g., Rabe et al. 2013). The water masses partly flow through the Nordic Seas to the Arctic Oceans and North Atlantic, respectively, partly mix at the Arctic front, or exchange with the interior basins (Mauritzen et al. 2011; Segtnan et al. 2011). Variability in the flux and characteristics of these water masses exists on a multitude of temporal and spatial scales (Skagseth et al. 2008) and cascades up through the ecosystem, impacting marine species (Hátun et al. 2009; Drinkwater 2011). This variability has resulted in a number of correlation studies in which time-series analyses have revealed periods of significant covariation between the physical environment and its inhabitants but break down during other periods (Ottersen et al. 2013). The response of marine organisms to ocean climate variability and change depends on the regularity of ocean climate variation and possible long-term trends. Abrupt changes, or changes beyond species-specific thresholds (Ottersen et al. 2013), may have severe effects on the development of the species abundance and distribution.

Several distinct, negative salinity anomalies, commonly termed Great Salinity Anomalies (GSAs), have been identified in the northeastern North Atlantic and downstream (northward) in the eastern Nordic Seas during the last 50 years. The most distinct GSAs appeared in the 1960s, late 1970s, mid-1980s, and mid-1990s (Dickson et al. 1988; Belkin et al. 1998; Belkin 2004; Sundby and Drinkwater 2007). The propagation time of these anomalies through the Nordic Seas has been estimated to be approximately 2 years from the Faroe-

---

Responsible Editor: Huijie Xue

---

This article is part of the Topical Collection on the *5th International Workshop on Modelling the Ocean (IWMO) in Bergen, Norway 17–20 June 2013*

---

**Electronic supplementary material** The online version of this article (doi:10.1007/s10236-014-0736-3) contains supplementary material, which is available to authorized users.

---

V. S. Lien (✉) · F. B. Vikebø  
Institute of Marine Research, Bergen, Norway  
e-mail: vidar.lien@imr.no

Y. Gusdal  
Meteorological Institute, Oslo, Norway

Shetland Channel to the Barents Sea Opening (BSO). These estimates are based on repeated hydrographic measurements at sections intercepting the main branches of the AW flowing northward. That propagation time corresponds to an advection speed of 0.02–0.03 m/s (Furevik 2001; Sundby and Drinkwater 2007). For comparison, this is approximately an order of magnitude less than the typical current speed in the Norwegian Atlantic Slope Current (NASC; Orvik et al. 2001). Generally, the temperature of the northward flowing AW varies in phase with the salinity (Furevik 2001). Thus, GSAs are also associated with anomalously low temperatures, although along-path atmospheric interaction affects the temperature and salinity differently.

Sundby and Drinkwater (2007) argued that the GSAs can be explained by perturbations in the balance between salt diffusion and salt transport along the boundaries of the northern North Atlantic. In the northeastern North Atlantic, the salinity decreases downstream (northward) from the Faroe-Shetland Channel towards the Arctic Ocean. Assuming a constant salt diffusion, a reduced (increased) volume transport through the Faroe-Shetland Channel causes a reduction (increase) in the downstream salt transport. This relationship explains why the advection speed of a GSA is much lower than the AW current speed. Moreover, Sundby and Drinkwater (2007) identified positive salinity anomalies and found that the anomalies tended to have larger advection speeds compared with negative anomalies. Sundby and Drinkwater (2007) attributed both positive and negative GSAs to large-scale forcing, such as the North Atlantic Oscillation (NAO; Hurrell 1995), which either spins up (positive NAO and positive salinity anomaly) or slows down (negative NAO and negative salinity anomaly) the AW circulation.

In this study, we assess a numerical ocean model's ability to capture variations in the AW flowing along the Norwegian continental shelf. We then use the model to investigate short-term oceanic responses to anomalies in the regional atmospheric circulation and compare these oceanic responses to the situation of passing GSAs. Anomalous hydrography could either be short-term responses to passing low-pressure systems or an adjustment to multi-year changes in the strength and location of atmospheric pressure systems (e.g., NAO, AO, and Scandinavian Pattern, see Bader et al. 2011), as indicated by Sundby and Drinkwater (2007). Similarities and differences between hydrographic anomalies associated with low-frequency GSAs and short-term upwelling/downwelling events are investigated in terms of vertical structure, horizontal extent, and duration. We argue that the short-term oceanic adjustments to transient changes in regional atmospheric circulation, although less durable than the GSAs, may play an important role in the ecosystem functioning. Our understanding of these processes and ability to distinguish between them in time-series analyses that relate climate signals to biological

effects has great implications for our general understanding of how marine species in the Nordic Seas ecosystem may respond to expected changes in their environment.

## 2 Data and methods

### 2.1 Ocean model

We utilize results from the Regional Ocean Modeling System (ROMS), a three-dimensional baroclinic ocean general circulation model that uses topography-following  $s$ -coordinates in the vertical (Shchepetkin and McWilliams 2005) and is coupled to an ice module (Budgell 2005). The model is implemented with a horizontal grid resolution of 4 km covering the Nordic, Barents, and Kara Seas as well as parts of the Arctic (Fig. 1). The model setup has 32 vertical  $s$ -coordinates and a minimum depth of 10 m. The advection scheme chosen for momentum and tracers are fourth-order centered and third-order upstream, respectively, with the harmonic horizontal mixing coefficient set to zero. The generic length-scale (GLS) mixing scheme (Umlauf and Burchard 2003; Umlauf et al. 2003) is used for the vertical turbulent mixing of momentum and tracers.

For atmospheric forcing, six-hourly values of winds, temperature, pressure, humidity, cloud cover, and accumulated precipitation from the Norwegian Reanalysis 10-km (NORA10) high-resolution archive (Reistad et al. 2011) are applied. Short- and net long-wave radiations are computed internally. The archive is a dynamic downscaling based on ERA40 (Uppala et al. 2005) for the period January 1958 to August 2002 and EC analysis from September 2002 and onward, producing atmospheric fields at a 10-km resolution. The archive covers most of the interior of the ocean model domain but has been expanded with ERA40 and EC analysis, respectively, in the boundary regions.

The Simple Ocean Data Assimilation data set (SODA; Carton et al. 2000; Carton and Giese 2008) and sea ice from a simulation using the ocean model MICOM (Sandø et al. 2012) are used as initial and boundary conditions by applying the boundary condition scheme proposed by Marchesiello et al. (2001). Tidal forcing based on a global ocean tides model (TPXO4) is included by imposing surface elevation and corresponding barotropic velocity components at the open boundaries, as proposed by Flather (1976) and Chapman (1985), respectively. Regarding freshwater input from rivers, the model uses monthly mean climatological values of river runoff. Interannual variability has been accounted for by scaling the climatological values based on precipitation extent from ERA40 and ERA Interim. The sea surface salinity is relaxed toward the SODA monthly mean values, with an e-folding time of 180 days to prevent drift in the model salinity. To account for model spin up, the first 2 years are neglected in

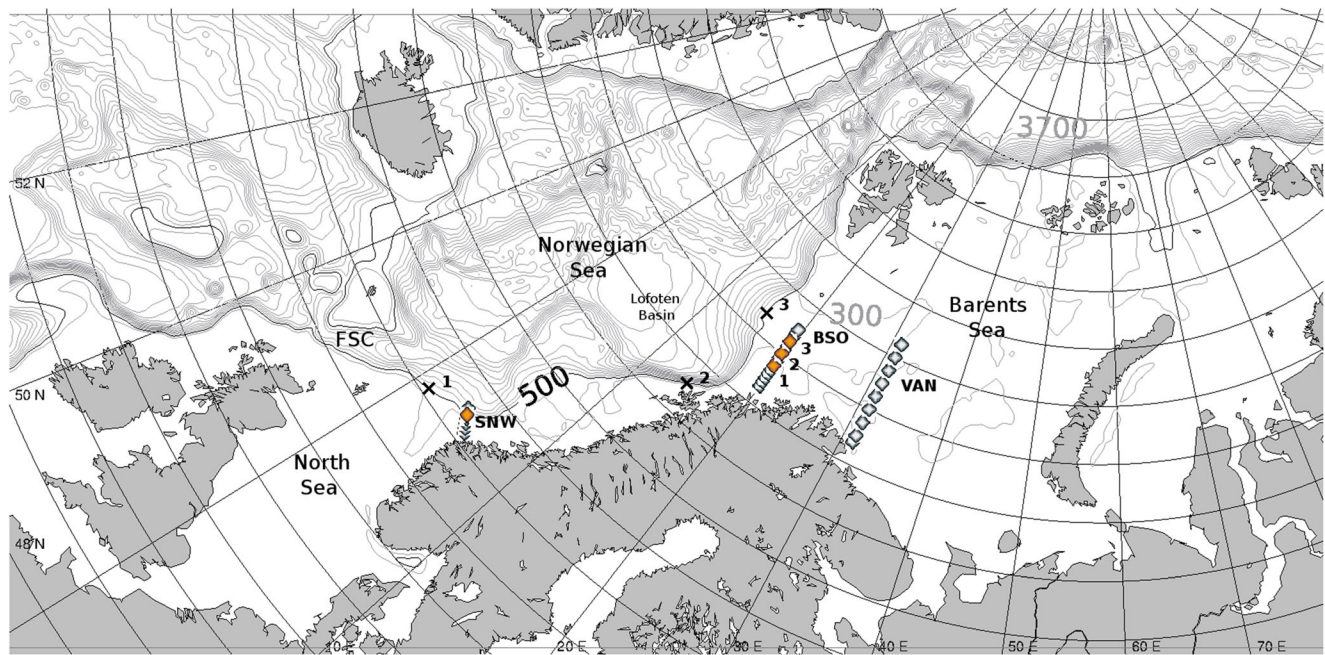


**Fig. 1** Model domain. The *gray contour lines* represent the bottom topography (with a minimum depth of 300 m). *Open squares* show the repeated sections: *SNW* Svinøy Northwest, *BSO* Barents Sea Opening,

*VAN* Vardø North. *Orange squares* show position of current meter measurements. *Crosses* show position of wind stations. *FSC* Faroe-Shetland Channel

the following analysis. For further details on the model simulation, see Lien et al. (2013a).

## 2.2 Observational data

Hydrographic data (temperature and salinity) from three repeated sections (Svinøy Northwest (SNW), the BSO, and the Vardø North (VAN); Fig. 1) are obtained from the Norwegian Marine Data Center database ([www.imr.no/forskning/faggrupper/norsk\\_marint\\_datasenter\\_nmd](http://www.imr.no/forskning/faggrupper/norsk_marint_datasenter_nmd)). To obtain an adequate data set for statistical calculations at each section, only 5-week periods containing observations at all stations within each section (Fig. 1) throughout the climatic period 1980–2009 are included in the analysis (see Kangas et al. 2006). The resulting measurement frequencies of the repeated sections are three times a year in the SNW, four times a year in the VAN, and six times a year in the BSO. Temperature and salinity anomalies are calculated for both the observations and the model results when observations are available and at observation station locations using the 30-year period 1980–2009 as a climatological normal period. The salinities and temperatures are spatially averaged within the AW, here defined by  $T > 3\text{ }^{\circ}\text{C}$  and  $S > 34.8$  between 50 and 200 m. This salinity criterion is below the value of 35.0 that is commonly used to define AW (e.g., Skagseth et al. 2008) to ensure a continuous time series during strong GSA events. In the SNW, we only include stations with a bottom depth of less than 1,000 m to focus on the NASC. In addition to the daily averages, modeled monthly temperature and salinity

anomalies relative to the climatological period 1980–2009 are calculated for the entire simulation period (Fig. 2).

Volume transport estimates from the SNW are based on hourly current meter data from a single current meter (Orvik and Skagseth 2003) for the period 1995–2011. The observations are filtered with a 30-day moving average and re-sampled every 15th day of each calendar month and compared with monthly mean model results. The model grid cell in the SNW section displaying the highest correlation with the observational time series is used for comparison with the observations. Note that the model grid cell with the largest modeled speed (i.e., representing the AW core) shows qualitatively similar results but with a slightly lower correlation. Correspondingly, current meter data in the BSO are processed into monthly averaged volume transport estimates for the period 1997–2011 (see, e.g., Ingvaldsen et al. 2004 for further details) and compared with the modeled volume transports of AW. In these calculations, we use the full section between Norway and Bear Island and define the AW by  $T > 3\text{ }^{\circ}\text{C}$  and  $S > 34.9$ , i.e., the salinity is adjusted for the model-observation bias/root mean square error (rmse) (Table 1). For the current speed comparison, the current meter data are processed into daily averages and compared with modeled daily averages at 50 m depth and at the bottom in BSO and at 100 m depth in the SNW. In the BSO, we only apply the observations in the central part of the section (Fig. 1) where the core of AW inflow occurs.

Additionally, we extract the along-slope wind component parallel to the 500 m isobath based on the NORA10 atmospheric data set at three locations along the Norwegian

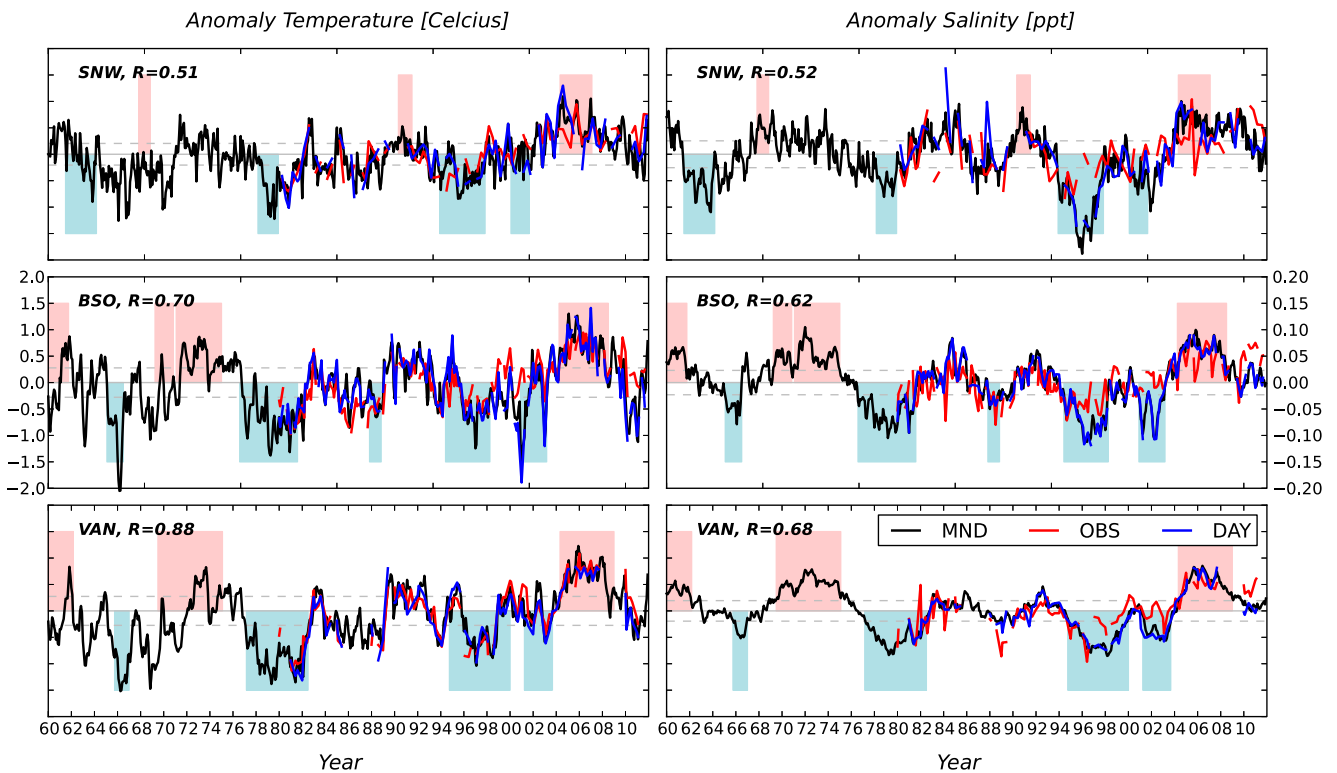


**Fig. 2** Time series of temperature (*left*) and salinity (*right*) anomalies in the core area of the Atlantic Water from modeled monthly averages (*black*), observations (*red*), and modeled daily averages at time of observations (*blue*). Base period is 1980–2009 with the seasonal variability

removed. *Top*, the Svinøy Northwest section; *middle*, the Barents Sea Opening; and *bottom*, the Vardø North section. *Horizontal lines* show 0.5 standard deviations. *Shaded areas* show periods of positive (*red*) and negative (*blue*) salinity anomalies within each section

continental shelf break (Fig. 1). The six-hourly time series of along-slope winds are smoothed by applying a 30-day moving average and re-sampled at the 15th of each calendar month. The along-slope wind component is then used as a proxy for the cross-slope Ekman transport and subsequent vertical displacement of the AW along the Norwegian continental slope (see Lien et al. 2013b).

To investigate the oceanic vertical response to atmospheric forcing, we compare the along-slope wind components described above and the monthly mean NAO index (Climate Analysis Section, NCAR, Boulder, USA; Hurrell et al. 2003) with the modeled maximum depth of the AW (defined by the 3 °C isotherm) along the continental slope limited by the 500- and 1,000-m isobaths. The difference of using, e.g., the 5 °C

isotherm is small (the depths of the 3 and 5 °C isotherms are highly correlated;  $R=0.94$ ;  $p<0.001$ ).

We define negative (positive) GSAs as periods of at least 12 consecutive months with a salinity anomaly more than 0.5 standard deviations below (above) the long-term mean (based on the modeled monthly time series shown in Fig. 2). Thus, we use the term “GSAs” for both negative and positive long-term anomalies. Negative (positive) regional wind-generated anomaly (RWA) are defined as months where the along-slope wind anomaly is more than 1.5 standard deviations below (above) the long-term mean. Thus, the RWAs are allowed to be of shorter durations than the GSAs and are therefore less likely to be observed based on repeated hydrographic sections with the sampling rate of today. By applying this definition,

**Table 1** Integrated values of bias and root mean square error (rmse) for temperature and salinity in the core area of the Atlantic Water from observations and daily average model results

Section	Bias		rmse	
	Temperature (°C)	Salt (ppt)	Temperature (°C)	Salt (ppt)
Svinøy Northwest section	-1.02	-0.11	1.27	0.14
Barents Sea Opening	-0.62	-0.09	0.79	0.10
Vardø North	-0.29	-0.07	0.55	0.08

The results cover the period 1980 to 2009 in the Svinøy Northwest section, the Barents Sea Opening, and the Vardø North section

the RWAs occupy approximately 10 % of the total time series (approximately 5 % positive and 5 % negative anomalies). To estimate the propagation time and speed of the modeled GSAs, we use the modeled AW salinity time series (by applying a 12-month moving average) at each section (Fig. 2). The propagation times and speeds are determined by identifying the time lag (months) that yields the maximum correlation for each individual GSA period.

In this study, we use the Pearson's correlation coefficient to compare various time series. For hydrography, we correlate de-seasoned and de-trended anomalies sampled a few times a year. For the AW depth, along-slope wind and the NAO index, we correlate monthly averages. The persistence of the NAO is typically less than a month (Barnes and Hartmann 2010); whereas, the along-slope winds are mainly driven by passing low-pressure systems (time scales of ~days). Therefore, the number of degrees of freedom in each time series is set to  $N-1$ , where  $N$  is the length of the time series or the sample size. The NAO index, AW depth, and the along-slope wind are neither de-seasoned nor de-trended prior to the correlation analysis.

### 3 Results

#### 3.1 Model evaluation

The modeled temperature and salinity at the three sections (SNW, BSO, and VAN) exhibit similar features of low-frequency variability on inter-annual to decadal timescales, as is evident from the observations (Fig. 2). Distinct maxima are present in the early 1960s, early 1970s, mid-1980s, early 1990s, and mid-2000s. Pronounced minima are observed during the mid-1960s, late 1970s, late 1980s, and mid-1990s, which is consistent with the chain of both positive and negative GSAs reported by Sundby and Drinkwater (2007). The most notable discrepancies are linked to the GSA during the mid-1990s and distinct modeled temperature and salinity anomalies during the early 2000s. A freshwater anomaly within the Nordic Seas in the mid-1990s has been documented (Carton et al. 2011). Although the model exaggerates the salinity anomaly associated with the GSA of the 1990s, the modeled temperature is close to the observed temperature during this period (Fig. 2). The modeled anomaly in the early 2000s has not, to our knowledge, been documented through observations presented in literature. There are at least two potential explanations for this discrepancy. First, consistent with the standard monitoring of AW properties (Blindheim and Loeng 1981), we use the 50- to 200-m depth range within the AW part of the sections to represent the AW core. Therefore, our analysis is sensitive to the vertical extent of the anomaly, which may differ in the model and in nature. Second, only including observations from 5-week periods a

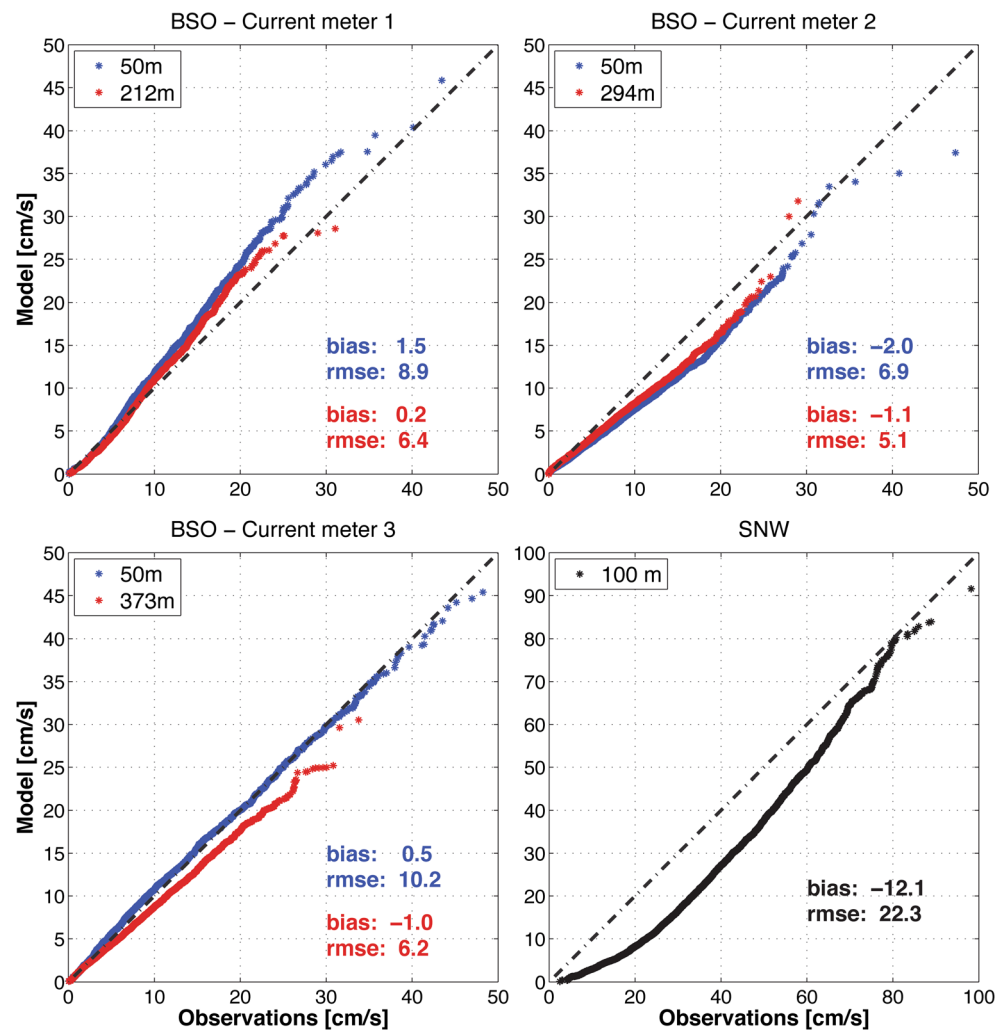
few times per year limits the temporal data coverage. The early 2000s is therefore not treated as a GSA, although it fulfills the definition given above, but is investigated in more detail in the following discussion.

Table 1 shows the bias and rmse between the observed and modeled salinity and temperature. The model has a negative bias that decreases downstream in both temperature and salinity in the repeated sections over the period 1980–2011,  $-0.11$  (SNW),  $-0.09$  (BSO), and  $-0.07$  (VAN) in salinity and  $-1.02$  (SNW),  $-0.62$  (BSO), and  $-0.29$  (VAN) in temperature. The corresponding rmse values also decrease downstream from 0.14 (SNW), 0.10 (BSO) to 0.08 (VAN) for salinity and 1.27 (SNW), 0.79 (BSO) to 0.55 (VAN) for temperature.

The correlations between modeled and observed temperature ( $R_T$ ) and salinity ( $R_S$ ) (Fig. 2) generally increase downstream from  $R_T=0.51$  and  $R_S=0.52$  in the SNW,  $R_T=0.70$  and  $R_S=0.62$  in the BSO, to  $R_T=0.88$  and  $R_S=0.68$  in the VAN ( $p<0.001$  for all values). The increasing correlations downstream reflect the better representation of variability also on shorter timescales (intra-annual to annual) in the Barents Sea compared with the Norwegian Sea. The correlation between the observed and modeled volume transport is  $R=0.63$  ( $p<0.001$ ) in the SNW. If the seasonal signal is removed, the correlation coefficient reduces to  $R=0.46$  ( $p<0.001$ ). In the BSO, the correlation is  $R=0.41$  ( $p<0.001$ ) while adjusting for the seasonal signal yields a correlation coefficient  $R=0.38$  ( $p<0.001$ ). The estimated net AW volume transports and standard deviations through the BSO for the period 1997–2011 are  $2.0\pm 1.0$  Sv and  $1.9\pm 1.0$  Sv for observations and model results, respectively. We find a close agreement between the observed and the modeled current speed distribution at a depth of 50 m and at the bottom in the BSO (Fig. 3). The model generally overestimates the current speeds with a bias of 1.5 cm/s at 50 m and 0.2 cm/s at the bottom at station 1, while at station 2, the model underestimates the current speeds with a bias of  $-2.0$  cm/s (50 m) and  $-1.1$  cm/s (bottom). At station 3, the model underestimates the current speeds at the bottom ( $-1.0$  cm/s) and slightly overestimates the current speeds at 50 m (0.5 cm/s). Upstream in the SNW, the model underestimates the observed current speeds (Lien et al. 2013a; Fig. 3) with a bias of  $-12.1$  cm/s. This discrepancy was attributed to possible differences in the bathymetry, as well as the problem of comparing a 4-by-4-km grid cell to point measurements when considering the narrow core of the NASC (10 km; Orvik et al. 2001). The rmse of the current speeds are between 5.1 and 6.4 cm/s at the bottom and between 6.9 and 10.2 cm/s at a depth of 50 m in the BSO and 22.3 cm/s at a depth of 100 m in the SNW.

According to Lien et al. (2013a), the modeled AW depth is realistic within the southern basin in the Norwegian Sea, although the vertical temperature and salinity gradients in the transition layer between the AW and the Norwegian Sea

**Fig. 3** Quantile–quantile plot (qq-plot) between daily average observed and modeled current speed at a depth of 50 m (*blue*) and at the bottom (*red*) in the Barents Sea Opening (*BSO*) and at a depth of 100 m (*black*) in the Svinøy Northwest section (*SNW*). For positions of the current meter moorings, see Fig. 1



Intermediate Water (NSIW) is weaker than observed. Compared with the observed heat content within the Nordic Seas (Skagseth and Mork 2012), the major part of the modeled heat content within the Nordic Seas is contained within the NASC at the expense of especially the Lofoten Basin (Lien et al. 2013a). Using ROMS with a similar setup, Isachsen et al. (2012) found too-small shelf-basin AW exchanges when investigating the surface eddy heat fluxes in the Lofoten Basin, which explains the lack of modeled heat within the interior Lofoten basin. For a further evaluation of the model performance, see Lien et al. (2013a).

### 3.2 Great salinity anomalies

The estimated GSA propagation speeds are summarized in Table 2. The results show different propagation speeds for the GSA60s (~0.02 m/s), GSA70s (~0.13 m/s), and GSA90s (~0.08 m/s) from the SNW to the BSO. The lesser modeled basin scale heat and freshwater inertia could be possible explanations for the larger modeled GSA propagation speeds, compared with the observation-based estimates of ~0.03 m/s

(Furevik 2001; Sundby and Drinkwater 2007). Between the BSO and the VAN, however, the estimated propagation speeds are in the range of 0.01–0.02 m/s for all three GSAs investigated. We identify two positive salinity anomalies that are simultaneously present in all three sections; one during the late 1960s and early 1970s and one during the mid-2000s (Fig. 2). The propagation speeds of these two differ considerably from the SNW to the BSO (0.04 and 0.17 m/s,

**Table 2** Propagation times (months) for the Great Salinity Anomalies between various sections, with corresponding propagation speed (m/s) in parenthesis

Section	SNW-BSO (~1,360 km)	BSO-VAN (~375 km)
GSA60s	27 (0.019)	10 (0.015)
GSA70s	4 (0.13)	7 (0.021)
GSA90s	7 (0.075)	11 (0.013)

The propagation time corresponds to the downstream time lag of the maximum correlation between the sections, with a 12-month moving average applied to the time series. Section names: Svinøy Northwest (SNW), Barents Sea Opening (BSO), and Vardø North (VAN)

respectively) but are consistently low from the BSO to the VAN (0.03 and 0.04 m/s, respectively). Thus, the proposed difference in propagation speeds between positive (faster) and negative (slower) anomalies, as proposed by Sundby and Drinkwater (2007), remains inconclusive based on this study.

### 3.3 Regional wind-generated anomalies

To investigate the relation between atmospheric forcing and dynamic response in the ocean, we look at the modeled maximum depth of the AW (represented by the 3 °C isotherm) and its covariation with the along-slope wind components (Fig. 4). Negative (positive) values of the along-slope wind anomaly favor offshore (onshore) Ekman transport and subsequently an ascending (descending) boundary layer between the warm and saline AW overlying the colder and less saline NSIW. Based on the monthly averages, we find significant correlations between the maximum depth of the AW and the along-slope wind both at station 1 ( $R=0.46$ ;  $p<0.001$ ) and at station 2 ( $R=0.43$ ;  $p<0.001$ ). If we use values of the along-slope wind anomaly that are outside the 1.5 standard deviation range only, the correlations increase to  $R=0.76$  ( $p<0.001$ ;  $N=79$ ) and  $R=0.63$  ( $p<0.001$ ;  $N=88$ ), respectively. At station 3, we find no significant correlation between the along-slope wind component and the maximum depth of the AW, neither for the entire model period nor for extreme values only. Considering the clearly coherent response in the maximum AW depth northward (Fig. 4; Supplementary Fig. S1), we extend our analysis to include the correlation between the along-slope wind at station 2 and the maximum AW depth at station 3. We then find a significant correlation ( $R=0.22$ ;  $p<0.001$ ) at zero time lag, increasing to  $R=0.35$  ( $p<0.001$ ) at 1-month time lag. For extreme values (outside  $\pm 1.5$  standard deviations;  $N=88$ ), we find a significant correlation of  $R=0.37$  ( $p<0.001$ ) at zero time lag, which increases to  $R=0.57$  ( $p<0.001$ ) at 1-month time lag.

Acknowledging that our along-slope wind represents the local atmospheric forcing, we continue by comparing the maximum depth of the AW with the large-scale atmospheric circulation represented by the NAO index. The NAO is representative for the large-scale atmospheric circulation and has been proposed as a driving mechanism for the GSAs (Sundby and Drinkwater 2007). The correlation between the monthly NAO index and the combined along-slope wind anomaly at stations 1 and 2 (as depicted in Fig. 4) is  $R=0.41$  ( $p<0.001$ ). We obtain correlations between the NAO index and the AW depth of  $R=0.35$  ( $p<0.001$ ) at station 1,  $R=0.49$  ( $p<0.001$ ) at station 2, and  $R=0.21$  ( $p<0.001$ ) at station 3 using monthly averages. Including extreme values of the NAO index only (i.e., outside 1.5 standard deviations of the long-term mean;  $N=73$ ) we obtain  $R=0.58$  ( $p<0.001$ ) at station 1,  $R=0.76$  ( $p<0.001$ ) at station 2, and  $R=0.49$  ( $p<0.001$ ) at station 3.

Clearly, there is a large temporal variability in the maximum depth of the AW at monthly to annual timescales (Fig. 4). On average, the maximum depth of the AW is approximately 500 m from the inflow area at 61° N to the BSO at approximately 71° N. The depth then rapidly decreases northward (Fig. 4). During periods of positive NAO and downwelling favorable along-slope winds, the AW may reach depths exceeding 700 m from the SNW to the Fram Strait. In contrast, during periods of negative NAO and upwelling-favorable along-slope winds, the AW is moved up to 200 m upslope (monthly average).

### 3.4 Great salinity anomalies versus regional wind-generated anomalies

Figure 5 shows the modeled temperature and salinity anomalies in the SNW and the BSO during months representing (1) GSAs (negative), (2) negative RWAs, (3) GSAs (negative) combined with negative RWAs, and (4) winter 2000/2001. The motivation for investigating winter 2000/2001 in more detail is the apparent GSA that occurs in the model but not in the observations. To account for the advection time from the continental slope to the BSO, a 1-month time lag is applied between the wind anomalies at station 2 and the hydrographic anomalies in the BSO in cases 2 and 3. To reduce the influence of RWAs on the GSAs and vice versa, months representing RWAs are omitted when compiling the GSAs. Similarly, months defined to be inside a GSA are omitted when compiling the RWAs. We then find that in the SNW, the GSAs are associated with a general reduction of both temperature and salinity within the AW. On the contrary, RWAs are associated with a subsurface reduction in temperature and salinity, mostly confined to the continental slope, and an increase/decrease in surface temperature/salinity (Fig. 5). This relationship is consistent with an uplift of the boundary layer between the NSIW and the overlying AW through offshore advection of warm and less saline coastal water in the surface layer. The relationship is further substantiated by the negative sea surface height anomaly along the coast during negative RWAs, pointing towards offshore Ekman transport (Fig. 5, bottom). During GSAs, we find no such pattern in the sea surface height anomaly.

In the BSO, the difference between the GSAs and the RWAs is less clear. Consistent with the findings in the SNW, there is a general cooling and freshening during GSAs. During months with negative RWAs, the salinity tends to be slightly higher than normal, while there is a weak cooling in the southern part of the section. Most notably, the anomalies in both temperature (negative) and salinity (positive) are most pronounced within the Norwegian Coastal Current. When combining all of the months that are found to be inside both a GSA and a RWA, there is a tendency of a negative, bottom-intensified anomaly in temperature. In salinity, there is also a

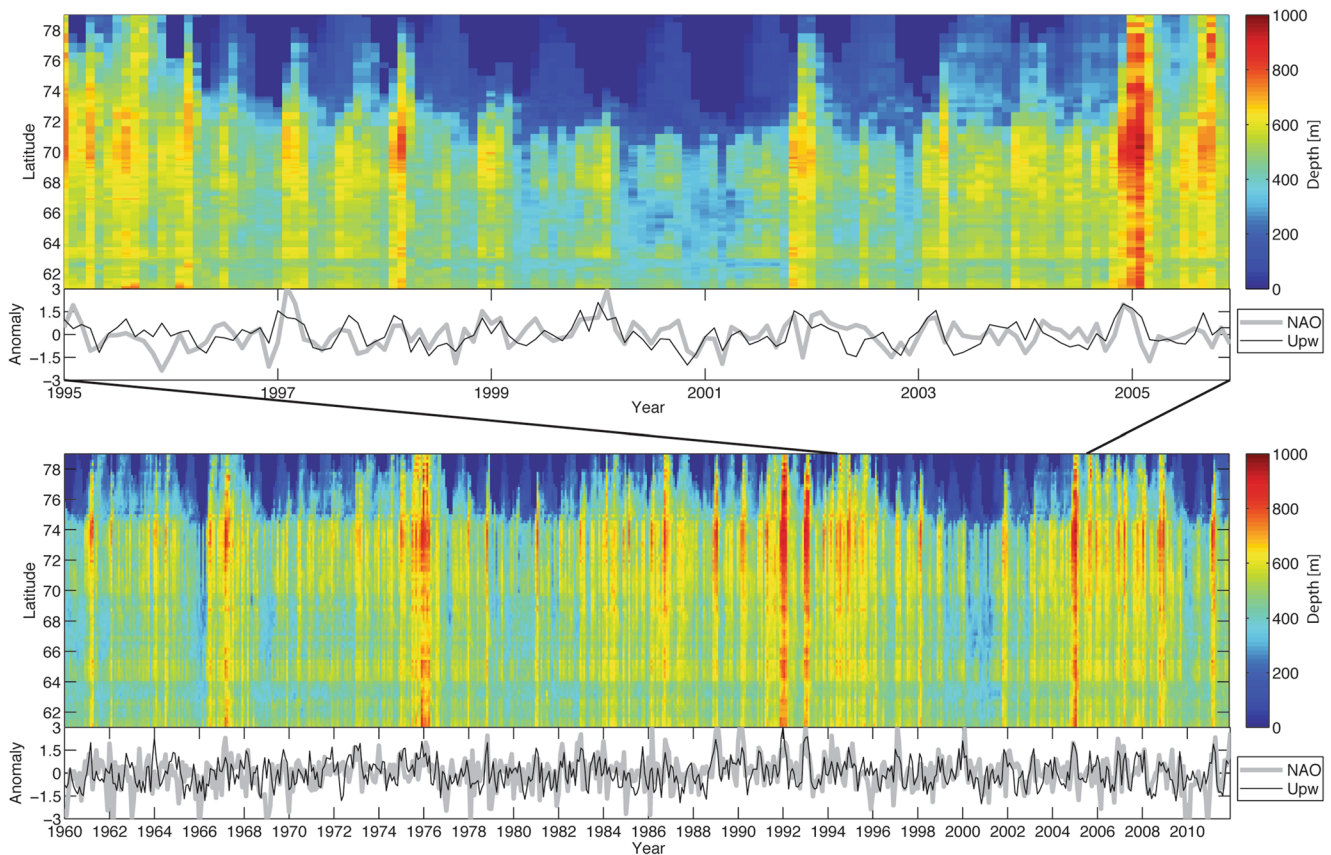


**Fig. 4** HovMöller diagram showing the depth in meters (*color*) of the 3 °C isotherm against time (*x*-axis) and latitude (*y*-axis). Time series show standardized anomalies of monthly NAO index (*thick, gray line*) and the

average along-slope wind at stations 1 and 2 (*Upw; black line*). *Bottom*, the whole simulation period; *top*, the years 1995–2005

general reduction throughout the section, but the strongest anomaly is located in the surface layer in the southern part of the section.

The temperature and salinity anomalies associated with the GSAs are more pronounced at a depth of 200 m compared with the anomalies associated with the RWAs, which are instead more pronounced at a depth of 400 m (Fig. 5). The 2000/2001 event especially displays a large anomaly in temperature at a depth of 400 m in the model.

### 3.5 2000/2001 anomaly

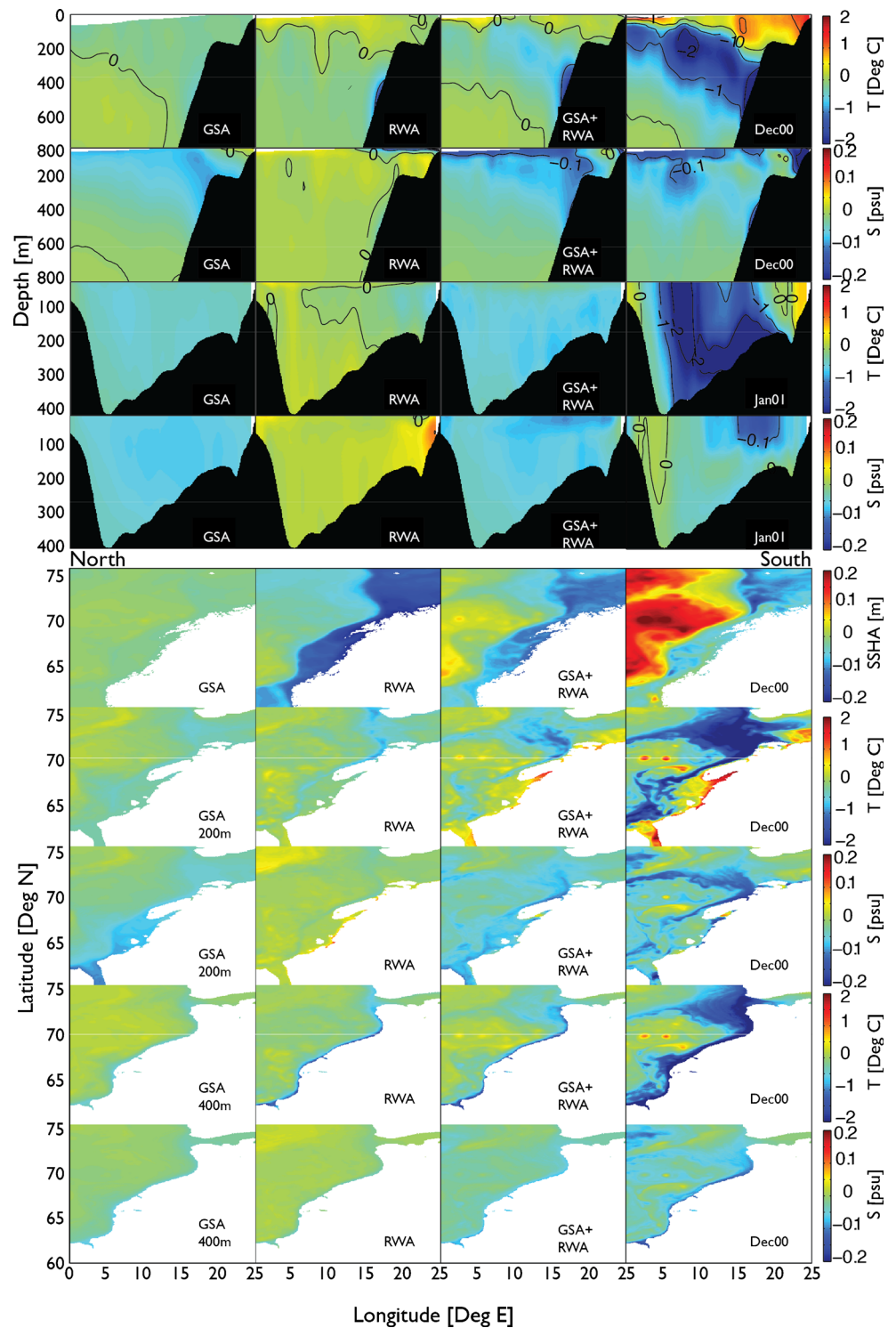
During winter 2000/2001, the depth of the 3 °C isotherm was displaced approximately 200 m upward from the SNW to the BSO and surfaced northward toward the Fram Strait (Fig. 4). As a consequence, the AW-NSIW boundary layer ascended above the bottom depth of the largest troughs, and NSIW-influenced water masses were transported onto the Norwegian continental shelf, including the western Barents Sea (Fig. 6). In the model, this occurrence is manifested as a negative, subsurface (200–600 m depth) temperature anomaly ( $|T_a| > 2$  °C) occurring simultaneously in the SNW and BSO sections (Fig. 5). As a consequence, the standard hydrography

monitoring procedure used here (covering only 50–200 m) likely miss at least part of the RWAs. To substantiate this, negative temperature ( $|T_a| = 2$  °C) and salinity ( $|S_a| = 0.1$ ) anomalies were observed in the SNW on 29 November 2000 (Supplementary Fig. S2). This observation is, however, outside the pre-defined 5-week periods included in our time series analysis. The anomalies were located somewhat deeper (300–600 m depth) and confined to the 1,000 m isobath (Supplementary Fig. S2) compared with the modeled anomalies (Fig. 5).

The bottom temperature anomaly depicted in Fig. 6 expands the modeled geographically coherent evolution of the hydrographic response to the wind-induced AW shoaling during winter 2000/01. The mean sea level pressure over the Norwegian Sea during the period October 2000 through May 2001 is shown in Supplementary Fig. S3 for comparison with the modeled oceanic response depicted in Fig. 6. Initially in October 2000, a negative temperature anomaly ( $|T_a| \sim 1$  °C) is observed along the path of the AW, bounded onshelf by the 300-m isobath. During November and December 2000, the along-path temperature anomaly intensifies and spreads onto shelf areas deeper than 300 m (200 m in the BSO). During the same months (Oct–Dec), there was anomalous low-pressure



**Fig. 5** Temperature (rows 1 and 3) and salinity (rows 2 and 4) anomalies in the Svinøy section (top) and the Barents Sea Opening (bottom). Far left shows anomalies during months defined as “Great Salinity Anomaly” months, but with along-slope winds less than 1.5 standard deviations outside the long-term average. Left shows anomalies in months when the along-slope wind is more than 1.5 standard deviations below average (i.e., northerly winds with shallow water to the left). Right shows anomalies during months defined as “Great Salinity Anomaly” months and when the along-slope wind is more than 1.5 standard deviations below average. Far right shows anomalies in December 2000 (Svinøy section) and January 2001 (Barents Sea Opening). West/north are to the left and east/south are to the right in the Svinøy Northwest and Barents Sea Opening, respectively. Bottom panel, Corresponding sea surface height anomalies (top), temperature (row 2) and salinity (row 3) anomalies at 200 m depth and temperature (row 4) and salinity (row 5) anomalies at 400 m depth. All the anomalies are relative to season



activity (Supplementary Fig. S3; anomalies are not shown) along the southern boundary of the Norwegian Sea, with an associated anomalous easterly component in the winds further north. By January 2001, a negative temperature anomaly  $|T_a| > 2 \text{ }^\circ\text{C}$  extends into all troughs and channels that are directly connected to the continental slope. At this stage, it is also evident that the temperature anomaly is advected eastward

through the BSO and into the northern parts of the BSO. During the period February through May 2001, the bottom temperature anomaly slowly becomes weaker. A similar evolution, but with positive temperature anomalies is found during the event of downwelling-favorable winds and subsequent deepening of the AW in winter 2004/2005 (Supplementary Fig. S4).

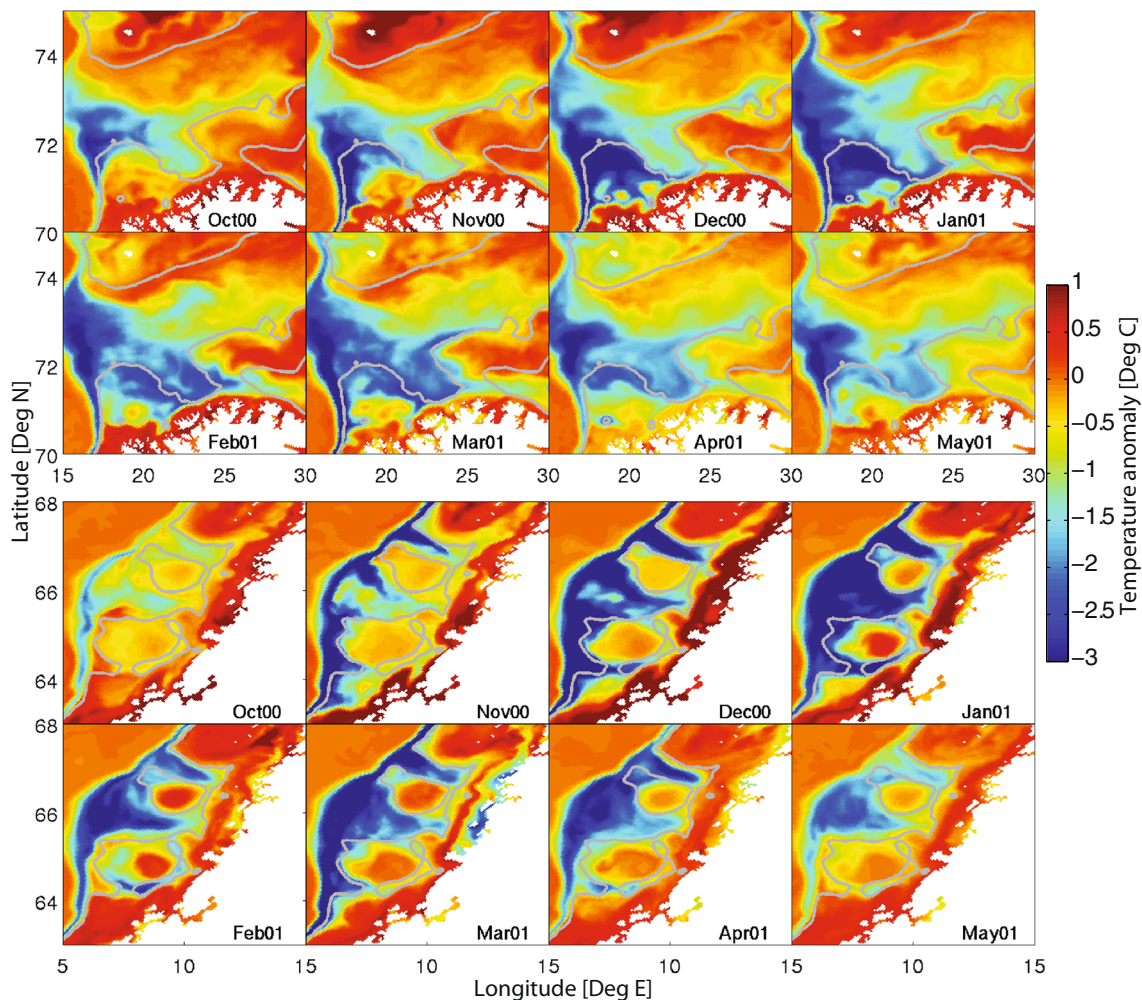


**Fig. 6** Temperature anomalies at the bottom during winter 2000/2001 (October through May). All anomalies are adjusted relative to season. The gray line depicts the 300-m isobath

#### 4 Discussion

The northward flow of warm and saline AW through the eastern Nordic Seas sustains a spring-bloom ecosystem hosting some of the world's largest commercial fish stocks. Although disentangling the different links from climate change and variation to responses in marine species is a major challenge, the focus in this study has been on the vertical structure, duration and propagation of salinity and temperature anomalies on the eastern side of the Nordic Seas. Large-scale temperature and salinity anomalies associated with GSAs may affect the thermal habitat within the Atlantic-dominated part of the Nordic Seas, whereas the dynamic response to changes in regional atmospheric forcing in addition affects the basin-shelf interaction. The latter has the potential to affect key processes in this relatively simple arcto-boreal spring-bloom ecosystem (Skjoldal 2004). One such process is the dispersal of *Calanus finmarchicus* onto shelves inhabited by the highly migratory Norwegian spring-spawning herring (*Clupea harengus*) and the Northeast Arctic cod (*Gadus morhua*),

whose offspring are dependent on the availability of early stages of *C. finmarchicus* (e.g., Sundby 2000). Therefore, understanding the mechanisms behind variability in the ocean projected onto proxy data is crucial for predicting the expected ecosystem response.

The ocean model successfully recaptures the main features of observed variability in AW temperature, salinity and volume transports, with episodic discrepancies. Specifically, all major GSAs (positive and negative) according to Sundby and Drinkwater (2007) are reproduced. Additionally, the BSO volume transport of AW, which is continuously monitored by five current meter moorings, is near identical in terms of the mean and standard deviation.

We have identified positive and statistically significant correlations between the depth of the AW along the upper continental slope in the Norwegian Sea and both the NAO index and the along-slope wind at zero time lag. Based on CTD measurements, Mork and Blindheim (2000) found a positive but weak correlation between the NAO in winter and the 100- to 400-m average temperature and salinity in

the SNW the following summer. Our study differs in that we compare monthly NAO with the modeled AW depth for the period 1960–2011, whereas Mork and Blindheim (2000) used winter-NAO and hydrographic observations from the period July/August 1978–1996. We interpret these results as the NAO and variability in the along-slope wind inducing transient responses in the upper-slope AW depth on timescales of a few months. Given the general intensification of the NAO during winter, either positive or negative, the anomalies in the AW depth are generally amplified during winter. Thus, the RWAs are more short lived and more frequent compared with the GSAs. While our model results suggest a total of six GSAs (four negative, including the 2000/2001 event, and two positive), during the 52-year period 1960–2011, we find annually occurring anomalies in the AW depth, although large amplitudes occur less frequently and usually in correspondence with large anomalies in the NAO and/or the along-slope wind.

Whereas the GSAs are well documented in literature (e.g., Dickson et al. 1988), the RWAs and their impacts are less well documented, although their origin is based on well-known atmosphere–ocean interactions. The general lack of observations at high spatiotemporal resolution is a likely explanation why reports of the RWAs are scarce. One source of observations at high temporal resolution is moored instruments. Anomalously low AW volume and heat transport was observed in the BSO during late winter 2001 (Skagseth et al. 2008, Fig. 2.6) based on an array of five oceanographic moorings. Although reduced current speeds through the BSO would have resulted in such an anomaly, a reduction in temperature and salinity would also create an anomaly in AW volume and heat transport due to the temperature- and salinity-dependent definition of AW. A two-degree temperature drop beginning in mid-December 2000 and persisting throughout the winter was recorded close to the bottom at mooring position 3 (Ingvaldsen, personal communication; see Fig. 1 for position), consistent with a modeled bottom-intensified temperature anomaly (Fig. 5). This result suggests a reduction in the amount of AW present in the BSO in favor of NSIW-influenced water masses because the AW-NSIW boundary layer is elevated within the mainly barotropic currents in the BSO. As for the SNW, the temperature and salinity anomalies are confined to the lower part of the water column and are not captured by the standard 50–200 m depth AW monitoring.

Figure 4 and Supplementary Fig. S1 suggest that the anomalies in the AW depth are occurring more or less simultaneously along the Norwegian continental slope (i.e., south of 70° N). This is consistent with the passing of high- or low-pressure systems, which traverse the area on a timescale of days. Based on daily averages of AW depth plotted against time and latitude (not shown), we find that the positive AW depth anomalies (downwelling) are propagating northward from station 2 at speeds approximately 0.1 to 0.4 m/s (propagation

of negative AW depth anomalies (upwelling) is less clear). This result is substantiated by the higher correlation between the AW depth at station 3 and the wind forcing at station 2 one month earlier, compared with the wind forcing at station 3 at no lag. A possible mechanism for such propagation is topographically trapped Kelvin waves, which can be expected to play a role in oceanic adjustment to changes in atmospheric forcing on timescales on the order of a few months and less (Primeau 2002; Marshall and Johnson 2013). Using an idealized model setup for the Nordic Seas basin, Yang and Pratt (2013) calculated a typical traveling speed of 0.9 m/s for a baroclinic Kelvin wave along the Nordic Seas rim, about three times the speed indicated in our model simulation, which corresponds to a propagation time of approximately 15 days from stations 2 to 3.

The modeled propagation speeds of 0.02–0.04 m/s between the BSO and the VAN for both the positive and negative GSAs as well as the 2000/01 anomaly event are comparable to the observed (Ingvaldsen et al. 2002) and modeled (Fig. 3; Lien et al. 2013a, b) mean current speed through the BSO. This result indicates plume advection of the temperature and salinity anomalies onto the shelf and is further substantiated by the damping of the amplitudes between the BSO and the VAN (Figs. 2, 6, and Supplementary Fig. S4). Contrary to a GSA, the wind-driven shoaling of the AW along the continental slope allows for more NSIW-influenced water masses to be advected onshelf through troughs. This mechanism has been identified as being important for the renewal of the water masses at the shelf (Connolly and Hickey 2014). Such water mass renewal impacts both the hydrographic properties and the exchange of tracers between the shelf and the open ocean. Thus, the renewal affects the thermal habitat and food availability of early stages of fish spawned at the shelf, such as the Norwegian spring-spawning herring (*C. harengus*) and Northeast Arctic cod (*G. morhua*). Moreover, the renewal may also contribute to replenishing the nutrients at the shelf. Therefore, wind-driven shoaling events potentially play important roles in the marine ecosystem functioning.

**Acknowledgments** This study has been supported by the Norwegian Research Council through the project PRIBASE (grant number 191698/S40) and SVIM (grant number 196685). Randi Ingvaldsen is acknowledged for preparing mooring data from the BSO and Kjell Arne Mork for providing Supplementary Fig. S2. The authors wish to thank two anonymous reviewers for comments that greatly improved the manuscript.

**Open Access** This article is distributed under the terms of the Creative Commons Attribution License which permits any use, distribution, and reproduction in any medium, provided the original author(s) and the source are credited.

## References

- Bader J, Mesquita MDS, Hodges KI, Keenlyside N, Østerhus S, Miles M (2011) A review on Northern Hemisphere sea-ice, storminess and the North Atlantic Oscillation: observations and projected changes. *Atmos Res* 101:809–834
- Barnes EA, Hartmann DL (2010) Dynamical feedbacks and the persistence of the NAO. *J Atmos Sci* 67:851–865
- Belkin IM (2004) Propagation of the “Great Salinity Anomaly” of the 1990s around the northern North Atlantic. *Geophys Res Lett* 31, L08306. doi:10.1029/2003GL019334
- Belkin IM, Levitus S, Antonov J, Malmberg S-A (1998) “Great Salinity Anomalies” in the North Atlantic. *Prog Oceanogr* 41:1–68
- Blindheim J, Loeng H (1981) On the variability of Atlantic influence in the Norwegian and Barents Seas. *Fiskdir Skr Ser Havunders* 17:161–189
- Budgell WP (2005) Numerical simulation of ice-ocean variability in the Barents Sea region: towards dynamical downscaling. *Ocean Dyn* 55:370–387
- Carton JA, Giese BS (2008) A reanalysis of ocean climate using simple ocean data assimilation (SODA). *Mon Weather Rev* 136:2999–3017
- Carton JA, Chepurin G, Cao X, Giese BS (2000) A simple ocean data assimilation analysis of the global upper ocean 1950–95. Part I: methodology. *J Phys Oceanogr* 30:294–309
- Carton JA, Chepurin GA, Reagan J, Häkkinen S (2011) Interannual to decadal variability of Atlantic Water in the Nordic and adjacent seas. *J Geophys Res* 116, C11035
- Chapman DC (1985) Numerical treatment of cross-shelf open boundaries in a barotropic coastal ocean model. *J Phys Oceanogr* 15:1060–1075
- Connolly TP, Hickey BM (2014) Regional impact of submarine canyons during seasonal upwelling. *J Geophys Res* 119. doi:10.1002/2013JC009452
- Dickson RR, Meincke J, Malmberg SA, Lee AJ (1988) The Great Salinity Anomaly in the Northern North-Atlantic 1968–1982. *Prog Oceanogr* 20:103–151
- Drinkwater KF (2011) The influence of climate variability and change on the ecosystems of the Barents Sea and adjacent waters: review and synthesis of recent studies from the NESSAS Project. *Prog Oceanogr* 90:47–61
- Flather RA (1976) A tidal model of the northwest European continental shelf. *Mem Soc Roy Sci Liege* 6(10):141–164
- Furevik T (2001) Annual and interannual variability of Atlantic Water temperatures in the Norwegian and Barents Seas: 1980–1996. *Deep-Sea Res I* 48:383–404
- Hansen B, Østerhus S (2000) North Atlantic–Nordic Seas exchanges. *Prog Oceanogr* 45:109–208
- Hátun H, Payne MR, Beaugrand G, Reid PC, Sandø AB, Drange H, Hansen B, Jacobsen JA, Bloch D (2009) Large bio-geographical shifts in the north-eastern Atlantic Ocean: from the subpolar gyre, via plankton, to blue whiting and pilot whales. *Prog Oceanogr* 80: 149–162
- Hurrell JW (1995) Decadal trends in the North-Atlantic Oscillation—regional temperatures and precipitation. *Science* 269:676–679
- Hurrell JW, Kushnir Y, Ottersen G, Visbeck M (Eds) (2003) The North Atlantic oscillation: climate significance and environmental impact. *Geophys Monogr Ser* 134:279pp
- Ingvaldsen R, Loeng H, Asplin L (2002) Variability in the Atlantic inflow to the Barents Sea based on a one-year time series from moored current meters. *Cont Shelf Res* 22:505–519
- Ingvaldsen R, Asplin L, Loeng H (2004) The seasonal cycle in the Atlantic transport to the Barents Sea during the years 1977–2001. *Cont Shelf Res* 24:1015–1032
- Isachsen PE, Koszalka I, LaCasce JH (2012) Observed and modeled surface eddy heat fluxes in the eastern Nordic Seas. *J Geophys Res* 117, C08020
- Kangas TV, Svendsen E, Strand Ø (2006) Normalverdier for saltholdighet og temperatur i Havforskningsinstituttets faste snitt. *Fisken og Havet* 6:53pp (in Norwegian)
- Lien VS, Gusdal Y, Albrechtsen J, Melsom A, Vikebø FB (2013a) Evaluation of a Nordic Seas 4 km numerical ocean model archive. *Fisken og Havet* 7:79 pp
- Lien VS, Vikebø FB, Skagseth Ø (2013b) One mechanism contributing to co-variability of the Atlantic inflow branches to the Arctic. *Nat Commun* 4:1488
- Marchesiello P, McWilliams JC, Shchepetkin A (2001) Open boundary conditions for long-term integration of regional oceanic models. *Ocean Model* 3:1–20
- Marshall DP, Johnson HL (2013) Propagation of meridional circulation anomalies along western and eastern boundaries. *J Phys Oceanogr* 43:2699–2717
- Mauritzen C, Hansen E, Andersson M, Berx B, Beszczynska-Möller A, Burud I, Christensen KH, Debernard J, de Steur L, Dodd P, Gerland S, Godøy Ø, Hansen B, Hudson S, Høydalsvik F, Ingvaldsen R, Isachsen PE, Kasajima Y, Koszalka I, Kovacs KM, Koltzow M, LaCasce J, Lee CM, Lavergne T, Lydersen C, Nicolaus M, Nilsen F, Nøst OA, Orvik KA, Reigstad M, Schyberg H, Seuthe L, Skagseth Ø, Skardhamar J, Skogseth R, Sperrevik A, Svensen C, Søiland H, Teigen SH, Tverberg V, Riser CW (2011) Closing the loop—approaches to monitoring the state of the Arctic Mediterranean during the International Polar Year 2007–2008. *Prog Oceanogr* 90:62–89
- Mork KA, Blindheim J (2000) Variations in the Atlantic inflow to the Nordic Seas, 1955–1996. *Deep-Sea Res I* 47:1035–1057
- Orvik KA, Skagseth Ø (2003) Monitoring the Norwegian Atlantic slope current using a single moored current meter. *Cont Shelf Res* 23:159–176
- Orvik KA, Skagseth Ø, Mork M (2001) Atlantic inflow to the Nordic Seas: current structure and volume fluxes from moored current meters, VM-ADCP and SeaSoar-CTD observations, 1996–1999. *Deep-Sea Res I* 48:937–957
- Ottersen G, Stige LC, Durant JM, Chan KS, Rouyer TA, Drinkwater KF, Stenseth NC (2013) Temporal shifts in recruitment dynamics of North Atlantic fish stocks: effects of spawning stock and temperature. *Mar Ecol Prog Ser* 480:205–225
- Primeau F (2002) Long Rossby wave basin-crossing time and the resonance of low-frequency basin modes. *J Phys Oceanogr* 32:2652–2665
- Rabe B, Dodd PA, Hansen E, Falck E, Schauer U, Mackensen A, Beszczynska-Möller A, Kattner G, Rohling EJ, Cox K (2013) Liquid export of Arctic freshwater components through the Fram Strait 1998–2011. *Ocean Sci* 9(1):91–109
- Reistad M, Breivik Ø, Haakenstad H, Aarnes OJ, Furevik BR, Bidlot JR (2011) A high-resolution hindcast of wind and waves for the North Sea, the Norwegian Sea, and the Barents Sea. *J Geophys Res Oceans* 116, C05019
- Sandø AB, Nilsen JEØ, Eldevik T, Bentsen M (2012) Mechanisms for variable North Atlantic–Nordic Seas exchanges. *J Geophys Res* 117, C12006
- Segtman OH, Furevik T, Jenkins AD (2011) Heat and freshwater budgets of the Nordic Seas computed from atmospheric reanalysis and ocean observations. *J Geophys Res* 116, C11003
- Shchepetkin AF, McWilliams JC (2005) The Regional Ocean Modeling System (ROMS): a split-explicit, free-surface, topography-following coordinates ocean model. *Ocean Model* 9:347–404
- Skagseth Ø, Mork KA (2012) Heat content in the Norwegian Sea, 1995–2010. *ICES J Mar Sci* 69(5):826–832. doi:10.1093/icesjms/fss026
- Skagseth Ø, Furevik T, Ingvaldsen R, Loeng H, Mork KA, Orvik KA, Ozhigin V (2008) Volume and heat transports to the Arctic Ocean via the Norwegian and Barents Seas. In: Dickson R, Meincke J,

- Rhines P (eds) Arctic Subarctic ocean fluxes: defining the role of the Northern Seas in climate. Springer, New York, pp 45–64
- Skjoldal HR (2004) The Norwegian Sea ecosystem. Tapir Academic Press, Trondheim, ISBN: 82-519-1841-3
- Sundby S (2000) Recruitment of Atlantic cod stocks in relation to temperature and advection of copepod populations. *Sarsia* 85:277–298
- Sundby S, Drinkwater K (2007) On the mechanisms behind salinity anomaly signals of the northern North Atlantic. *Prog Oceanogr* 73: 190–202
- Umlauf L, Burchard H (2003) A generic length-scale equation for geophysical turbulence models. *J Mar Res* 61:235–265
- Umlauf L, Burchard H, Hutter K (2003) Extending the k-omega turbulence model towards oceanic applications. *Ocean Model* 5:195–218
- Uppala S et al (2005) The ERA-40 re-analysis. *Q J R Meteorol Soc* 131: 2961–3012
- Yang J, Pratt LJ (2013) On the effective capacity of the dense-water reservoir for the Nordic Seas overflow: some effects of topography and wind stress. *J Phys Oceanogr* 43:418–431